

A simplified approximate analytical model for Rayleigh–Taylor instability in elastic–plastic solid and viscous fluid with thicknesses

Xi Wang(王曦)[1], Xiao-Mian Hu(胡晓棉)[1], Sheng-Tao Wang(王升涛)[1], and Hao Pan(潘昊)[1,2,†]

Citation: Chin. Phys. B, 2021, 30 (**4**): 044702. DOI: 10.1088/1674-1056/abcf44
Journal homepage: http://cpb.iphy.ac.cn; http://iopscience.iop.org/cpb

What follows is a list of articles you may be interested in

Effects of heat loss and viscosity friction at walls on flame acceleration and deflagration to detonation transition

Jin Huang(黄金), Wenhu Han(韩文虎), Xiangyu Gao(高向宇), Cheng Wang(王成)
Chin. Phys. B, 2019, 28 (**7**): 074704. DOI: 10.1088/1674-1056/28/7/074704

Experimental investigation on underwater drag reduction using partial cavitation

Bao Wang(王宝), Jiadao Wang(汪家道), Darong Chen(陈大融), Na Sun(孙娜), Tao Wang(王涛)
Chin. Phys. B, 2017, 26 (**5**): 054701. DOI: 10.1088/1674-1056/26/5/054701

Numerical investigation of the interaction of the turbulent dual-jet and acoustic propagation

Yi-Ming Li(李一明), Bao-Kuan Li(李宝宽), Feng-Sheng Qi(齐凤升), Xi-Chun Wang(王喜春)
Chin. Phys. B, 2017, 26 (**2**): 024701. DOI: 10.1088/1674-1056/26/2/024701

Pseudopotential multi-relaxation-time lattice Boltzmann model for cavitation bubble collapse with high density ratio

Ming-Lei Shan(单鸣雷), Chang-Ping Zhu(朱昌平), Cheng Yao(姚澄), Cheng Yin(殷澄), Xiao-Yan Jiang(蒋小燕)
Chin. Phys. B, 2016, 25 (**10**): 104701. DOI: 10.1088/1674-1056/25/10/104701

Effect of noncircular orifice plates on the near flow field of turbulent free jets

Xu Min-Yi, Tong Xing-Qing, Yue Dan-Ting, Zhang Jian-Peng, Mi Jian-Chun, Nathan G. J., Kalt P. A. M.
Chin. Phys. B, 2014, 23 (**12**): 124703. DOI: 10.1088/1674-1056/23/12/124703

A simplified approximate analytical model for Rayleigh–Taylor instability in elastic–plastic solid and viscous fluid with thicknesses*

Xi Wang(王曦)[1], Xiao-Mian Hu(胡晓棉)[1], Sheng-Tao Wang(王升涛)[1], and Hao Pan(潘昊)[1,2,†]

[1] *Institute of Applied Physics and Computational Mathematics, Beijing* 100094, *China*
[2] *Center for Applied Physics and Technology, Peking University, Beijing* 100871, *China*

(Received 31 August 2020; revised manuscript received 29 October 2020; accepted manuscript online 1 December 2020)

A simplified theoretical model for the linear Rayleigh–Taylor instability of finite thickness elastic–plastic solid constantly accelerated by finite thickness viscous fluid is performed. With the irrotational assumption, it is possible to consider viscosity, surface tension, elasticity or plasticity effects simultaneously. The model considers thicknesses at rigid wall boundary conditions with the velocity potentials, and deals with solid elastic–plastic transition and fluid viscosity based on the velocity continuity and force equilibrium at contact interface. The complete analytical expressions of the amplitude motion equation, the growth rate, and the instability boundary are obtained for arbitrary Atwood number, viscosity, thicknesses of solid and fluid. The thicknesses effects of two materials on the growth rate and the instability boundary are discussed.

Keywords: Rayleigh–Taylor instability, viscosity, plasticity, thicknesses effects

PACS: 47.20.Ma, 66.20.–d, 46.35.+z, 68.55.jd **DOI:** 10.1088/1674-1056/abcf44

1. Introduction

The Rayleigh–Taylor instability (RTI) is ubiquitous when denser material lays above lighter one in gravitational field, or denser one is accelerated by the lighter one.[1–6] RTI in solids is dramatically determined by the nonlinear constitutive relation of elastic–plastic (EP) mechanical properties. Barnes' pioneer experiment performed that the perturbation growth was apparently governed by yield strength of EP solid.[7] In addition, the instability evolution is dependent on both the perturbation wavelength and the initial perturbation amplitude of the interface, which was noticed by Drucker[8] and subsequently confirmed by Barnes' later experiment.[9] The complex mechanical behaviors of RTI in solids are far from sufficiently understood for present.

The RTI in solids plays a great role in many physics research area, such as of relevance in geophysics, astrophysics, high energy density physics, and the inertial confinement fusion (ICF).[10–16] The problem especially causes attention because it can be a test experimental tool to evaluate yield strength and other mechanical properties of solid slab under extremely high strain and high strain rate conditions.[10,17–19] Furthermore, the solid accelerated by the melted metal layer generates RTI phenomena in experiments, such as, magnetically imploded liners[12,20,21] and the Laboratory Planetary Sciences experiment.[22–25] The EP mechanical transition of solid, viscosity of melted metal, thicknesses, and densities of two materials in the realistic experiments are usually concurrent and unavoidable. Those physical behaviors boost the complication of the theoretical analysis of RTI evolution.

For the purposes of comprehending the RTI in solids, several theoretical description models for the instability evolution have been developed, including the model based on energy balance, the normal modes method, the model based on the Newtonian second law, and the velocity composition method.

A firstly model based on energy balance was developed by Miles,[26] then followed by Robinson and Swelge,[27] for EP solid slab and vacuum interface with realistic physics meaning, but lacking sufficiently accuracy and underestimating the growth rate[28] and difficult to contain other effects such as viscosity, surface tension, and thicknesses of two materials.

The traditional normal modes method has been only applied into perfectly elastic solids[3,29,30] and it is too mathematically complex to treat the strength behavior of solid material to obtain analytical results. Although, inspired by Mikaelian,[31] Colvin replaced surface tension term with a shear modulus dependent term in elastic regime and expressed yield strength as effective lattice viscosity after plastic transition,[17,19] this method is still controversial in interpreting experiments.[32,33]

Furthermore, a model based on the Newtonian second law can simply consider different forces acting on the perturbed interface, such as surface tension, viscosity, elasticity, plasticity, *etc*.[34–38] Yet, the model is merely established for two semi-infinite thicknesses media.

With the velocity composition, Sun improved the accu-

*Project supported by of the Science Challenge Project of China (Grant No. TZ2018001).
†Corresponding author. E-mail: pan_hao@iapcm.ac.cn
© 2021 Chinese Physical Society and IOP Publishing Ltd

racy of approximate solutions of the growth rates for a semi-infinite solid–solid interface and solid–fluid interface but with the assumption of elastic solid.[39] Besides, Sun only showed the dispersion relation of the elastic solid slab with arbitrary thickness accelerated in a semi-infinite rarefied inviscid region.[39] In addition, Piriz obtained the stability boundaries by using the Helmholtz decomposition in the elastic phase, following Drucker[8] and the method of the limit analysis to treat rigid-plastic phase.[40] But, only solid accelerated by semi-infinite idea fluid is discussed. The composition method has not been performed to solid slab with plastic mechanical properties leading to different methods used in elastic and plastic regimes.

The representative RTI system, that finite-thickness solid with EP properties is accelerated by finite-thickness fluid with viscosity, is rarely studied by the previous theoretical models, which prevents the thorough interpretations of RTI in solids. Therefore, RTI between finite-thickness EP solid and finite-thickness viscous fluid, which is much closer to experimental conditions, is concentrated on. The goal of the present work is to illustrate a simplified approximate analytical method for RTI with relatively easy mathematical treatment and the convenient extension potential.

In this study, a simplified RTI linear analysis model for EP solid and viscous fluid both with arbitrary thicknesses and densities is performed. The primary idea of the model with the irrotational velocity potentials, which were used in fluids,[41] is presented and the reasonability for the simplification is shown in Section 2. In Section 3, previous approximate dispersion relation with viscosity and surface tension in finite-thicknesses fluids is obtained again by the model. Then, in Section 4, the analytical equation of perturbation amplitude evolution for EP solid and viscous fluid both with arbitrary thicknesses and densities, that can cover the early results of semi-infinite cases which were in excellent agreements with two-dimensional simulations,[36–38] is achieved. Moreover, the corresponding growth rate (in Subsection 4.1) and instability boundaries (in Subsection 4.2) are derived. The effects of thicknesses of two materials are discussed in the results in Subseection 4.3.

2. Analytical model

Figure 1 gives RTI features of two immiscible materials with the heavier one of density ρ_1 lying above on the lighter one of density ρ_2 at constant accelerator g which has opposite direction to y axis. Materials 1 and 2 have the thicknesses of h_1 and h_2 respectively. The materials are separated by $y = 0$ at initial moment.

For the RTI system with viscosity, surface tension, elasticity, the forces acting on the interface will depend on the perturbed velocity field determined by the momentum conservation equations. The velocity field can be decomposed into irrotational and rotational parts expressed by the velocity potentials and the stream functions as Bellman and Pennington did.[41] Because the forces at the interface generate the rotation of the flow field, the velocity decomposition method is hard to directly extend to the plastic regime of solid to obtain analytical results due to the nonlinear constitutive relation with EP transition. In order to deal with the complex RTI system which is closer to realistic situation, a simplification is made below.

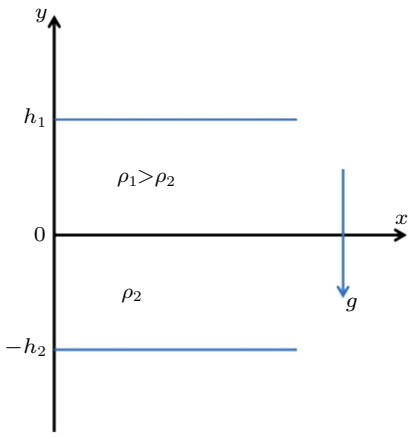


Fig. 1. Schematic diagram of the physical model.

In this work, the velocity field of the flow is assumed to be irrotational and expressed by the velocity potentials. The irrotational flow simplification is reasonable as mentioned in Ref. [42], that the vorticity generated by the forces acting on the interface only affects the velocity field for the wave number smaller than the associated vorticity mode, but RTI is rather insensitive to the velocity field for the smallest values of the wave number and the interface approaches the classical behavior. Besides, it needs to be emphasized that, with the perfect plastic assumption, the displacement field must be irrotational.[43] Although the accuracy may be reduced by the simplification, it is possible to deal with more complex situation with effects of EP transition, viscosity, and arbitrary thicknesses of two materials simultaneously. With the approximation, the analytical results can be achieved including the evolution of the perturbation amplitude, the growth rate, and the stability boundary for the interface of arbitrary thickness EP solid and arbitrary thickness viscous fluid in Section 4. The analytical expressions can cover the Piriz's semi-infinite results which are in excellent agreement with two-dimensional simulations.[36–38]

In the irrotational field, the momentum equations in two-dimensional Cartesian coordinates for incompressible materials are shown below:

$$\rho_i \frac{\partial \boldsymbol{u}_i}{\partial t} = -\nabla p_i + F_{ci}, \tag{1}$$

where the index i is 1, 2 representing materials 1 and 2. $\boldsymbol{u}_i$ represents the irrotational perturbed velocity of material i, p_i is the pressure and F_{ci} denotes the external conservative body force which equals $-\rho g$ in y direction for an acceleration field. $\boldsymbol{u}_i$ in the irrotational field can be expressed by velocity potential ϕ_i

$$\boldsymbol{u}_i = \nabla\phi_i, \tag{2}$$

ϕ_i for two materials with finite thicknesses have the following forms:[39,44]

$$\phi_1 = A_1(t)\,\mathrm{e}^{-ky}\cos kx + B_1(t)\,\mathrm{e}^{ky}\cos kx, \tag{3a}$$
$$\phi_2 = A_2(t)\,\mathrm{e}^{ky}\cos kx + B_2(t)\,\mathrm{e}^{-ky}\cos kx. \tag{3b}$$

where $A_i(t)$ and $B_i(t)$ have the form $\sim \mathrm{e}^{nt}$ where n is the growth rate. By combining the boundary conditions at $y = h_1$ and $y = -h_2$ when both materials are attached to a rigid side wall,

$$v_1(y = h_1) = \left.\frac{\partial\phi_1}{\partial y}\right|_{y=h_1} = 0,$$
$$v_2(y = -h_2) = \left.\frac{\partial\phi_2}{\partial y}\right|_{y=-h_2} = 0, \tag{4}$$

where v_1 and v_2 are the vertical velocities of materials, the velocity potentials turn into

$$\phi_1 = A_1(t)\left(\mathrm{e}^{-ky} + \mathrm{e}^{-2h_1k+ky}\right)\cos kx, \tag{5a}$$
$$\phi_2 = A_2(t)\left(\mathrm{e}^{ky} + \mathrm{e}^{-2h_2k-ky}\right)\cos kx. \tag{5b}$$

The initial interface $y = 0$ is perturbed by infinitesimal disturbance

$$\eta(x,t) = \xi(t)\cos kx, \tag{6}$$

where $k = 2\pi/\lambda$ is the wave number of the perturbation surface in x direction, λ is the perturbed interface wavelength, and $\xi(t)$ is the perturbation amplitude. Similarly to the way done in Ref. [39], by integrating Eq. (1) from $y = 0$ to the interface $y = \eta(x,t)$ and substituting velocity expression Eq. (2) into the integrated equation, the formulation of p_i can be written as

$$\begin{aligned} p_i &= p_i|_{y=0} + F_{ci,y}\eta - \rho_i\int_0^\eta \frac{\partial u_{i,y}}{\partial t}\,\mathrm{d}y \\ &= p_i|_{y=0} + F_{ci,y}\eta - \rho_i\int_0^\eta \frac{\partial^2\phi_i}{\partial t\partial y}\,\mathrm{d}y \\ &= p_i|_{y=0} + F_{ci,y}\eta - \rho_i\frac{\partial\phi_i}{\partial t} + \rho_i\left.\frac{\partial\phi_i}{\partial t}\right|_{y=0} \\ &= -\left(\rho_i g\eta + \rho_i\frac{\partial\phi_i}{\partial t} + C_i\right), \end{aligned} \tag{7}$$

At the initial state we have $y = \eta(x,0) = 0$ and the interface is in approximate equilibrium, then $C_1 = C_2$ can be obtained.

At the interface, the continuity of velocities and force equilibrium along the y direction need to be satisfied at any instantaneous time. The interface motion can be controlled by the normal velocity continuity equation

$$\frac{\partial\eta}{\partial t} = \frac{\partial\phi_1}{\partial y} = \frac{\partial\phi_2}{\partial y} \tag{8a}$$

and the normal force equilibrium

$$p_1 - p_2 + \sum_j F_y^{(j)} = 0 \tag{8b}$$

to the first order approximation. $F_y^{(j)}$ denotes the force acting on the two sides of per unitary interface in the vertical direction, such as, viscosity, surface tension, elasticity, or plasticity. Next, the physical analytical model will be used in RTI systems in different materials.

3. Finite-thicknesses fluids with viscosity and surface tension

The model is first applied to the RTI system of two finite thicknesses viscous fluids with surface tension to claim the reasonability of the methodology.

Based on the velocity continuity at the perturbation interface in Eq. (8a), the correlations of the interface amplitude $\xi(t)$ and the velocity potential factors $A_1(t)$ in Eq. (5a) and $A_2(t)$ in Eq. (5b) can be obtained

$$\dot{\xi}(t) = -kA_1(t)\left(1 - \mathrm{e}^{-2h_1k}\right) = kA_2(t)\left(1 - \mathrm{e}^{-2h_2k}\right). \tag{9}$$

And, there is the normal force equilibrium at the material interface according to Eq. (8b), *i.e.*

$$p_1 - S_{1,yy}^{(v)} - \left(p_2 - S_{2,yy}^{(v)}\right) - f_y^{(\mathrm{st})} = 0, \tag{10}$$

where $S_{i,yy}^{(v)}$ is, respectively, the vertical component of the deviatoric part of the Cauchy stress tensor $\sigma_{ij} = -p\delta_{ij} + S_{ij}$[44] for each fluid, and $f_y^{(\mathrm{st})}$ denotes the effect of surface tension.

For the Newtonian fluid at each side of the interface, the strain rate tensors are shown below:

$$D_{1,ij} = \frac{1}{2}\left(\frac{\partial u_{1,i}}{\partial x_j} + \frac{\partial u_{1,j}}{\partial x_i}\right) = A_1(t)\,\mathrm{e}^{-ky}k^2\begin{bmatrix} -\left(1+\mathrm{e}^{-2h_1k+2ky}\right)\cos kx & \left(1-\mathrm{e}^{-2h_1k+2ky}\right)\sin kx \\ \left(1-\mathrm{e}^{-2h_1k+2ky}\right)\sin kx & \left(1+\mathrm{e}^{-2h_1k+2ky}\right)\cos kx \end{bmatrix}, \tag{11a}$$

$$D_{2,ij} = \frac{1}{2}\left(\frac{\partial u_{2,i}}{\partial x_j} + \frac{\partial u_{2,j}}{\partial x_i}\right) = A_2(t)\,\mathrm{e}^{ky}k^2\begin{bmatrix} -(1+\mathrm{e}^{-2h_2k-2ky})\cos kx & -(1-\mathrm{e}^{-2h_2k-2ky})\sin kx \\ -(1-\mathrm{e}^{-2h_2k-2ky})\sin kx & (1+\mathrm{e}^{-2h_2k-2ky})\cos kx \end{bmatrix}. \tag{11b}$$

Then, because the deviatoric stress tensors have the forms of

$$S_{1,ij}^{(v)} = 2\mu_1 D_{1,ij}, \tag{12a}$$

$$S_{2,ij}^{(v)} = 2\mu_2 D_{2,ij}, \tag{12b}$$

where μ_1 and μ_2 are the dynamic viscosities of fluids 1 and 2 respectively, we can get the vertical components of stresses produced by viscosity:

$$S_{1,yy} = 2\mu_1 k^2 A_1(t)\,\mathrm{e}^{-ky}\left(1+\mathrm{e}^{-2h_1k+2ky}\right)\cos kx, \tag{13a}$$

$$S_{2,yy} = 2\mu_2 k^2 A_2(t)\,\mathrm{e}^{ky}\left(1+\mathrm{e}^{-2h_2k-2ky}\right)\cos kx. \tag{13b}$$

The effect of surface tension at the interface is performed by the Young–Laplace equation

$$f_y^{(\mathrm{st})} = \frac{T_{\mathrm{st}}}{R}, \tag{14}$$

where T_{st} is the surface tension coefficient and R is the local curvature radius which has the expression of

$$R = \left[1+\left(\frac{\partial\eta}{\partial x}\right)^2\right]^{3/2} \Big/ \frac{\partial^2\eta}{\partial x^2} \approx -\frac{1}{k^2\eta}, \quad k\eta \ll 1. \tag{15}$$

By substituting Eqs. (7), (13a), (13b), and (14) into Eq. (10), we obtain the motion equation of the interface amplitude $\xi(t)$ at $y=0$

$$\ddot{\xi} + 2k^2\frac{\mu_1\coth(h_1k)+\mu_2\coth(h_2k)}{\rho_1\coth(h_1k)+\rho_2\coth(h_2k)}\dot{\xi} + \frac{k^3T_{\mathrm{st}}-gk(\rho_1-\rho_2)}{\rho_1\coth(h_1k)+\rho_2\coth(h_2k)}\xi = 0, \tag{16}$$

whose dispersion relation of the growth rate is exactly the same as the approximate result of the dispersion relation formula Eq. (25) in Ref. [31] performed by Mikaelian who started from the general eigenvalue equation[46] by the classical normal modes analysis and then substituted the exact eigenfunctions for the inviscid case directly.

4. Solid slab and finite-thickness fluid interface

Next, material at $y>0$, below which viscous fluid of finite-thickness domain is still maintained, is changed to be solid slab with thickness h_1. The relations of the interface amplitude and the velocity potential factors can be derived as the similar way by combining the interface velocity continuity principal. The expression is uniform with Eq. (9).

By keeping equilibrium of the forces at the material interface, we have

$$p_1 - S_{1,yy}^{(\mathrm{ep})} - \left(p_2 - S_{2,yy}^{(v)}\right) = 0 \tag{17}$$

for EP solid and viscous fluid, where $S_{1,yy}^{(\mathrm{ep})}$ is the vertical component of the deviatoric stress in the elastic or plastic regime.

For a linear elastic solid (a Hookean solid),[47] the deviatoric stress tensor can be written as

$$\dot{S}_{1,ij} = 2G_1 D_{1,ij}, \tag{18a}$$

$$D_{1,ij} = \frac{1}{2}\left(\frac{\partial u_{1,i}}{\partial x_j}+\frac{\partial u_{1,j}}{\partial x_i}\right), \tag{18b}$$

where G_1 is the shear modulus of solid slab. By evaluating the velocity potential Eq. (5a), the rate of deformation tensor $D_{1,ij}$ in the y direction becomes

$$D_{1,yy} = A_1(t)\,\mathrm{e}^{-ky}k^2\left(1+\mathrm{e}^{-2h_1k+2ky}\right)\cos kx. \tag{19}$$

By giving the interface profile $\eta(x,0)=\xi_0\cos kx$ at initial time and integrating Eq. (18a) with Eq. (9), we obtain the deviatoric stress tensor

$$S_{1,ij} = -\frac{2G_1k(\xi-\xi_0)\,\mathrm{e}^{-ky}}{1-\mathrm{e}^{-2h_1k}} \times\begin{bmatrix} -\left(1+\mathrm{e}^{-2h_1k+2ky}\right)\cos kx & \left(1-\mathrm{e}^{-2h_1k+2ky}\right)\sin kx \\ \left(1-\mathrm{e}^{-2h_1k+2ky}\right)\sin kx & \left(1+\mathrm{e}^{-2h_1k+2ky}\right)\cos kx \end{bmatrix}, \tag{20}$$

and the vertical component in the elastic regime is

$$S_{1,yy}^{(\mathrm{ep})} = -2G_1k(\xi-\xi_0)\,\mathrm{e}^{-ky}\frac{1+\mathrm{e}^{-2h_1k+2ky}}{1-\mathrm{e}^{-2h_1k}}\cos kx. \tag{21}$$

Therefore, after substituting Eq. (21) into Eq. (17), we have

$$\ddot{\xi} + \frac{2\mu_2k^2\coth(h_2k)}{\rho_1\coth(h_1k)+\rho_2\coth(h_2k)}\dot{\xi} - \frac{gk(\rho_1-\rho_2)}{\rho_1\coth(h_1k)+\rho_2\coth(h_2k)}\xi = -\frac{2G_1k^2\coth(h_1k)}{\rho_1\coth(h_1k)+\rho_2\coth(h_2k)}(\xi-\xi_0). \tag{22}$$

When the effective stress arrives at the yield strength Y, *i.e.*,

$$\bar{\sigma} = \sqrt{\tfrac{3}{2}S_{1,ij}S_{1,ij}} = Y, \tag{23}$$

the solid slab will transient from elastic to plastic regime. By substituting the deviatoric stress tensor Eq. (21) into the effective stress, we have the specific expression below:

$$\bar{\sigma}^2 = \frac{3}{2}S_{1,ij}S_{1,ij} = 6G_1^2k^2(\xi-\xi_0)^2 \times\{\cos(2kx)+\cosh[2k(h_1-y)]\}\left[\mathrm{csc}\,h(h_1k)\right]^2. \tag{24}$$

As mentioned in Refs. [34,36], the solid mass in the thickness of k^{-1} from the interface affect the evolution of RTI motion. Here, the transition is assumed to take place until $y=k^{-1}$ bulks of material become plastic flow, which implies that the model is suitable for the case of $kh>1$. Considering $\cosh(2kh-2)\gg 1$ in most situations, the perturbation amplitude ξ_p at the time when the EP transition occurs is derived into

$$\xi_p - \xi_0 \approx \frac{Y\sinh(h_1k)}{\sqrt{6}G_1k\sqrt{\cosh(2h_1k-2)}}. \tag{25}$$

Thus, by combining the elastic branch in Eq. (22), the amplitude growth equation for EP solid slab accelerated by finite thickness viscous fluid is

$$\ddot{\xi}+\frac{2\mu_2k^2\coth(h_2k)}{\rho_1\coth(h_1k)+\rho_2\coth(h_2k)}\dot{\xi}-\frac{gk(\rho_1-\rho_2)}{\rho_1\coth(h_1k)+\rho_2\coth(h_2k)}\xi$$
$$=\begin{cases}-\dfrac{2G_1k^2\coth(h_1k)}{\rho_1\coth(h_1k)+\rho_2\coth(h_2k)}(\xi-\xi_0), & \xi\le\xi_p,\\ -\sqrt{\dfrac{2}{3}}\dfrac{\cosh(h_1k)}{\sqrt{\cosh(2h_1k-2)}}\dfrac{kY}{\rho_1\coth(h_1k)+\rho_2\coth(h_2k)}, & \xi\ge\xi_p.\end{cases}\tag{26}$$

The motion equation can describe the solid/fluid RTI system with arbitrary Atwood number, arbitrary thicknesses of both materials, dynamic viscosity, shear modulus and yield strength. Compared to the two fluids RTI case of Eq. (16) which is irrelevant with ξ_0, the evolution of interface is controlled by the initial perturbation amplitude ξ_0 that is typical characteristic in solid which is found by Drucker[8] and confirmed by Barnes' experiment.[9] Furthermore, the thicknesses multiplied by wave number as a factor act on the densities of both mediums that will influence the perturbation growth rate and instability boundary as shown below.

If $h_1k\gg1$ and $h_2k\gg1$, *i.e.* the semi-infinite solid and semi-infinite fluid domain, equation (26) becomes to be

$$\ddot{\xi}+\frac{2\mu_2k^2}{\rho_1+\rho_2}\dot{\xi}-\frac{\rho_1-\rho_2}{\rho_1+\rho_2}gk\xi$$
$$=\begin{cases}-\dfrac{2G_1k^2}{\rho_1+\rho_2}(\xi-\xi_0), & \xi\le\xi_p,\\ -\dfrac{e}{\sqrt{3}}\dfrac{kY}{\rho_1+\rho_2}, & \xi\ge\xi_p.\end{cases}\tag{27}$$

When the interface of semi-infinite solid is accelerated by rarefied inviscid gas, *i.e.*, $\rho_2=0$ and $\mu_2=0$, the motion equation turns into:

$$\ddot{\xi}-gk\xi=\begin{cases}-\dfrac{2G_1k^2}{\rho_1}(\xi-\xi_0), & \xi\le\xi_p,\\ -\dfrac{e}{\sqrt{3}}\dfrac{kY}{\rho_1}, & \xi\ge\xi_p.\end{cases}\tag{28}$$

Equations (27) and (28) whose analytical instability boundary results showed excellent agreements with numerical simulations were previously obtained by the method established by Piriz.[36–38]

4.1. The dispersion relations

From the amplitude evolution of solid slab and finite-thickness fluid interface in Eq. (26), it is convenient to obtain the analytical expression of the dispersion relation for the growth rate n for the plastic regime:

$$n^2+\frac{2\mu_2k^2\coth(h_2k)}{\rho_1\coth(h_1k)+\rho_2\coth(h_2k)}n$$
$$-\frac{gk(\rho_1-\rho_2)}{\rho_1\coth(h_1k)+\rho_2\coth(h_2k)}=0,\quad \xi\ge\xi_p.\tag{29}$$

Here, the dimensionless growth rate σ, wave number κ, thickness and viscosity are introduced

$$\sigma=\frac{n}{g}\sqrt{\frac{G_1}{\rho}},\quad \kappa=\frac{2G_1k}{\rho_1g},$$
$$\hat{h}_i=\frac{h_i\rho_1g}{2G_1},\quad D_0=\frac{\mu_2g}{2\sqrt{2}}\sqrt{\frac{\rho_1}{G_1^3}},\tag{30}$$

and the equation for the dimensionless growth rate σ is

$$\sigma^2+\frac{\sqrt{2}D_0\kappa^2\coth(\hat{h}_2\kappa)}{\coth(\hat{h}_1\kappa)+\frac{1-A_T}{1+A_T}\coth(\hat{h}_2\kappa)}\sigma$$
$$-\frac{\kappa\frac{A_T}{1+A_T}}{\coth(\hat{h}_1\kappa)+\frac{1-A_T}{1+A_T}\coth(\hat{h}_2\kappa)}=0,\quad \xi\ge\xi_p,\tag{31}$$

where $A_T=(\rho_1-\rho_2)/(\rho_1+\rho_2)$.

4.2. Stability boundary

Following the method in Refs. [37,38], the steps of deducing stability boundary are described below.

By introducing the following dimensionless variables:

$$z=\frac{\xi}{\xi_0},\quad \tau=t\sqrt{kg},\quad \hat{\lambda}=\frac{\rho_1g\lambda}{4\pi G_1},\quad \hat{\xi}=\frac{\rho_1g\xi_0}{\sqrt{3}Y},\tag{32}$$

the motion Eq. (26) reads

$$\ddot{z}+2D\dot{z}=\begin{cases}\Lambda-(\Lambda-\Omega)z, & z\le z_p,\\ \Omega z-X, & z\ge z_p,\end{cases}\tag{33}$$

where the symbols are defined as follows:

$$D=\frac{D_0}{\hat{\lambda}^{3/2}}\frac{\coth\left(\hat{h}_2/\hat{\lambda}\right)}{\coth\left(\hat{h}_1/\hat{\lambda}\right)+\frac{1-A_T}{1+A_T}\coth\left(\hat{h}_2/\hat{\lambda}\right)},\tag{34a}$$

$$\Omega=\frac{2A_T}{1+A_T}\cdot\frac{1}{\coth\left(\hat{h}_1/\hat{\lambda}\right)+\frac{1-A_T}{1+A_T}\coth\left(\hat{h}_2/\hat{\lambda}\right)},\tag{34b}$$

$$\Lambda=\frac{1}{\hat{\lambda}}\frac{\coth\left(\hat{h}_1/\hat{\lambda}\right)}{\coth\left(\hat{h}_1/\hat{\lambda}\right)+\frac{1-A_T}{1+A_T}\coth\left(\hat{h}_2/\hat{\lambda}\right)},\tag{34c}$$

$$X=\frac{\cosh\left(\hat{h}_1/\hat{\lambda}\right)}{\sqrt{\cosh\left(2\hat{h}_1/\hat{\lambda}-2\right)}}\frac{\sqrt{2}}{3\hat{\xi}}$$
$$\times\frac{1}{\coth\left(\hat{h}_1/\hat{\lambda}\right)+\frac{1-A_T}{1+A_T}\coth\left(\hat{h}_2/\hat{\lambda}\right)}.\tag{34d}$$

In addition, for the elastic–plastic transition, we have

$$\Lambda-(\Lambda-\Omega)z_p=\Omega z_p-X, \tag{35a}$$

$$z_p=\frac{X}{\Lambda}+1=\frac{\sqrt{2}\hat{\lambda}\sinh\left(\hat{h}_1/\hat{\lambda}\right)}{3\hat{\xi}\sqrt{\cosh\left(2\hat{h}_1/\hat{\lambda}-2\right)}}+1, \tag{35b}$$

and the corresponding initial conditions are

$$z(0)=1,\quad \dot{z}(0)=0. \tag{36}$$

To obtain the instability threshold, it is noticed that if the interface is stable, there will be a maximum perturbation amplitude $z(\tau)$ at a certain time τ_m. Hence, one must have $\dot{z}(\tau_m)=0$ and $\ddot{z}(\tau_m)\le 0$. The marginal stability should be determined by[36,46]

$$\dot{z}\left(\tau_m^{\rm th}\right)=0,\quad \ddot{z}\left(\tau_m^{\rm th}\right)=0. \tag{37}$$

For the domain of $z\le z_p$ and by introducing the transformation of

$$x_1=[\Lambda-(\Lambda-\Omega)z]\,{\rm e}^{D\tau},\quad z\le z_p, \tag{38}$$

the first branch of Eq. (33) can be transformed into

$$\ddot{x}_1=\left[D^2-(\Lambda-\Omega)\right]x_1,\quad z\le z_p, \tag{39}$$

and the initial conditions are

$$x_1(0)=\Omega,\quad \dot{x}_1(0)=D\Omega. \tag{40}$$

By integrating Eq. (39) for the first time with the initial conditions, we have

$$\dot{x}_1=-\sqrt{(D^2-(\Lambda-\Omega))x_1^2+(\Lambda-\Omega)\Omega^2},\quad z\le z_p, \tag{41}$$

where the negative sign is taken because of satisfying $z\ge 0$, $\dot{z}=0$, and $\ddot{z}\le 0$. By performing the second time integration from $\tau=0$ to the time $\tau_p^{\rm th}$ when the marginal stable state transits to the plastic regime, which has the boundary condition of $x_1(\tau_p^{\rm th})=x_p^{\rm th}$, we obtain

$$\tau_p^{\rm th}=-\frac{1}{\sqrt{D^2-(\Lambda-\Omega)}}\left(\sinh^{-1}\left(\sqrt{\frac{D^2-(\Lambda-\Omega)}{\Lambda-\Omega}}\frac{x_p}{\Omega}\right)-\sinh^{-1}\left(\sqrt{\frac{D^2-(\Lambda-\Omega)}{\Lambda-\Omega}}\right)\right). \tag{42}$$

With the condition of

$$\dot{x}_1\left(\tau_p^{\rm th}\right)=\dot{x}_{1p}^{\rm th}, \tag{43}$$

at the time $\tau_p^{\rm th}$, equation (41) can be written as

$$\dot{x}_{1p}^{\rm th}=-\sqrt{(D^2-(\Lambda-\Omega))\left(x_p^{\rm th}\right)^2+(\Lambda-\Omega)\Omega^2},\quad z\le z_p. \tag{44}$$

Similarly, with the transformation of

$$x_2=(\Omega z-X)\,{\rm e}^{D\tau},\quad z\ge z_p \tag{45}$$

in the $z\ge z_p$ domain, the second branch of Eq. (33) can become

$$\ddot{x}_2=\left(D^2+\Omega\right)x_2,\quad z\ge z_p. \tag{46}$$

Combining the initial conditions

$$x_2\left(\tau_p^{\rm th}\right)=x_p^{\rm th},\quad \dot{x}_2\left(\tau_p^{\rm th}\right)=\dot{x}_{2p}^{\rm th}, \tag{47}$$

and performing integration once of Eq. (46), we obtain

$$\dot{x}_2^2=\left(\dot{x}_{2p}^{\rm th}\right)^2+\left(D^2+\Omega\right)\left[x_2^2-\left(x_p^{\rm th}\right)^2\right]. \tag{48}$$

As equation (37) must be satisfied on the stability boundary, it has

$$x_2\left(\tau_m^{\rm th}\right)=\dot{x}_2\left(\tau_m^{\rm th}\right)=0, \tag{49}$$

with the second branch of Eq. (33) and the derivative of Eq. (45). Thus, equation (48) reads

$$\dot{x}_{2p}^{\rm th}=-\sqrt{D^2+\Omega}x_p^{\rm th}. \tag{50}$$

Then, by taking the first derivatives of Eqs. (38) and (45) and evaluating them at $\tau=\tau_p^{\rm th}$, and combining Eqs. (44) and (50), we obtain the expression for $x_p^{\rm th}$

$$x_p^{\rm th}=-\frac{\Omega^2}{\sqrt{\left(\Omega+2D\left(D+\sqrt{D^2+\Omega}\right)\right)\Lambda}}. \tag{51}$$

At the time $\tau=\tau_p^{\rm th}$, it has

$$x_p^{\rm th}=[\Lambda-(\Lambda-\Omega)z_p]\,{\rm e}^{D\tau_p^{\rm th}} \tag{52}$$

from Eq. (37). Then, according to the expression of z_p in Eq. (35b), the instability threshold can be derived to be

$$\frac{\rm X}{\Lambda}=\frac{\Omega-x_p^{\rm th}\,{\rm e}^{-D\tau_p}}{\Lambda-\Omega}, \tag{53}$$

which can be rewritten as

$$\hat{\xi}=\frac{\sqrt{2}\hat{\lambda}\sinh\left(\hat{h}_1/\hat{\lambda}\right)}{3\sqrt{\cosh\left(2\hat{h}_1/\hat{\lambda}-2\right)}}\cdot\frac{\Lambda-\Omega}{\Omega-x_p^{\rm th}\,{\rm e}^{-D\tau_p}} \tag{54}$$

with the definition of X and Λ in Eqs. (34d) and (34c). In the stability boundary equation, $\tau_p^{\rm th}$ and $x_p^{\rm th}$ are determined by Eqs. (34b), (34b), and (34c) in terms of D, Ω, Λ which are functions of the dimensionless wavelength $\hat{\lambda}$.

4.3. Results and discussions

4.3.1. Growth rate

The dimensionless growth rate $\sigma(\kappa)$ in the plastic regime is determined by the dispersion relation Eq. (31) which is a quadratic polynominal formula and always has real root. In Eq. (31), the solid yield strength does not affect the growth rate because of perfectly plasticity assumption that the yield strength is irrelevant to the strain after EP transition. Only the viscosity effect D_0 of fluid is left.

The dimensionless growth rates σ varying with the dimensionless wave number κ for the plastic solid slab are given in Fig. 2. σ increase to a peak value then decrease to asymptotic value as κ going to infinity. Figure 2(a) gives the growth rate *versus* wave number of disparate value of the dimensionless viscosity $D_0 = 2$, 1, 0.5 from bottom to top for fluid with $A_T = 0.5$ and $\hat{h}_1 = \hat{h}_2 = 1$. As expected, when the viscosity is boosted, the growth rates move downwards integrally in Fig. 2(a) and the asymptotic values as $\kappa \to \infty$ also decrease. The stabilization effect of the viscosity gets strong with viscosity increasing.

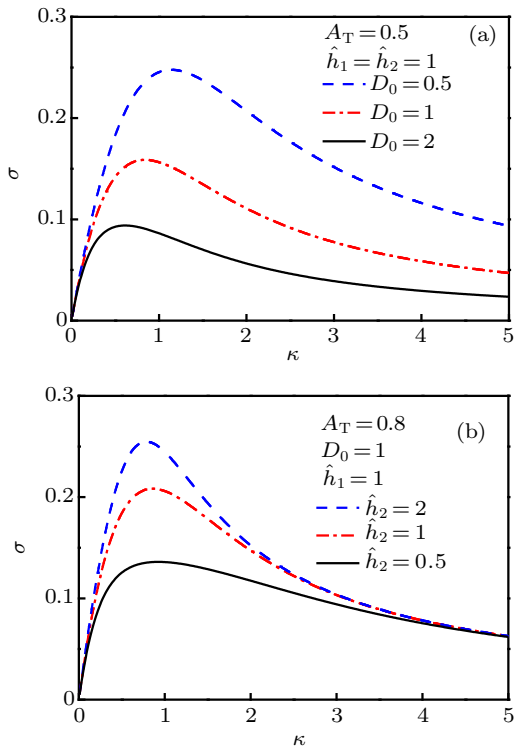


Fig. 2. The σ *versus* κ for the case of plastic-regime solid slab and finite-thickness viscous fluid. (a) $D_0 = 2$, 1, and 0.5 from bottom to top with $A_T = 0.5$ and $\hat{h}_1 = \hat{h}_2 = 1$; (b) $\hat{h}_2 = 0.5$, 1, and 2 from bottom to top with $\hat{h}_1 = 1$, $D_0 = 1$, and $A_T = 0.8$.

Figure 2(b) exhibits the comparison of three values of the dimensionless thicknesses for fluid with $\hat{h}_2 = 0.5$, 1, and 2 from bottom curve to top one respectively with $\hat{h}_1 = 1$, $D_0 = 1$, and $A_T = 0.8$. When fluid becomes thinner, the growth rate decreases and the system is more stable. The fluid thickness effect acting on the growth rate is more significant around $\kappa \approx 1$, but decreases with increasing wave number to a same asymptotic value.

4.3.2. Instability boundary

Instability boundaries for different situations given by the analytical expression in Eq. (54) are shown below. The instability boundary separates $\hat{\xi}$ *versus* $\hat{\lambda}$ domain into the upper unstable and lower stable area.

Figure 3(a) compares the instability boundaries between the present model and model result in Ref. [36]. A good match is obtained except for a little difference. The reason for the difference between the two results is that an approximation to ξ_p was made in Ref. [36] to get a better fit with the numerical simulation results.[36] Figure 3(b) gives the instability boundaries derived with present model for the interface of EP solid slab and vacuum by fixing $A_T = 1$ and $D_0 = 0$ and changing the value of $\hat{h}_1$ as ∞, 2, 1, and 0.5 from bottom curve to the top one. And decreasing the thickness of solid slab diminishes the unstable area and stabilizes the system for long wavelength situations.

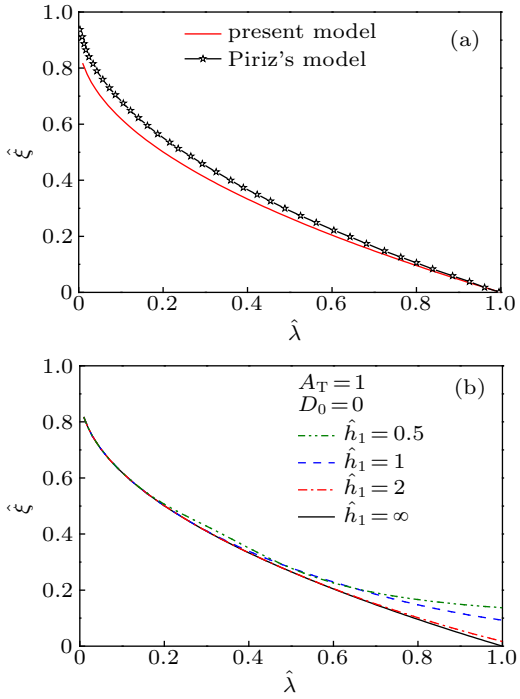


Fig. 3. The $\hat{\xi}$ as a function of $\hat{\lambda}$ for the instability boundaries at the solid slab and the semi-infinite inviscid fluid interface. (a) The bottom instability boundary is derived from the present model and the top one is the result in Ref. [36] when $\hat{h}_1 = \infty$, $A_T = 1$, and $D_0 = 0$; (b) $\hat{h}_1 = \infty$, 2, 1, and 0.5 from bottom to top with A_T =1 and D_0 = 0.

Figure 4(a) shows two groups of stability boundaries that the lower group is for $A_T = 0.8$ and the upper group is for $A_T = 0.2$. As expected, decreasing Atwood number is to enlarge the stable area. Increasing the density of the lighter material can prevent the growth of perturbation. In each group, different values 0, 0.01, 0.1, and 1 for dimensionless viscosity from bottom curve to top one respectively with $\hat{h}_1 = \hat{h}_2 = 1$ are presented. Piriz defined $D = D_0/\hat{\lambda}^{3/2}$, that is different from

definition in Eq. (34) which has a parameter relevant to the thicknesses and Atwood number of materials, when deducing the instability boundary for two semi-infinite domain of EP solid and viscous fluid.[37,38] Therefore, compared to the results of instability boundaries in Refs. [37,38], the thicknesses and A_T of the RTI system change the shape of the instability boundary, such as, for $D_0 = 1$ the instability boundary is not a straight line but convexes upwards at $A_T = 0.2$. Besides, the stabilizing effect when increasing viscosity is intense for low A_T than for high A_T.

Figure 4(b) performs the comparison of three thicknesses $\hat{h}_2 = 2$, 1, and 0.5 of lighter material from bottom to top with $A_T = 0.2$, $D_0 = 0.1$, and $\hat{h}_1 = 1$. The stable area is slightly enlarged as the density of lighter material becomes thinner. The thickness of light material mainly affects the growth rate of the RTI system as shown in Fig. 2(b).

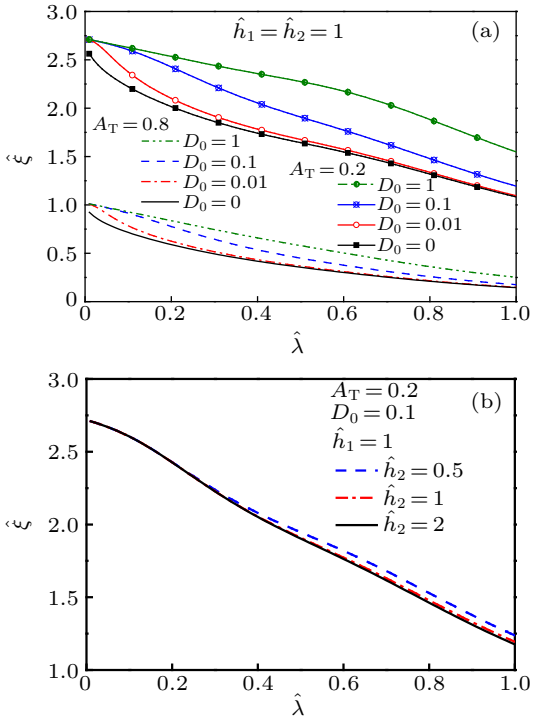


Fig. 4. The $\hat{\xi}$ as a function of $\hat{\lambda}$ for the instability boundaries at the solid slab and finite-thickness viscous fluid interface. (a) $D_0 = 0$, 0.01, 0.1, and 1 from bottom to top for lower group of $A_T = 0.8$ and upper group of $A_T = 0.2$ with $\hat{h}_1 = \hat{h}_2 = 1$; (b) $\hat{h}_2 = 2$, 1, and 0.5 from bottom to top with $A_T = 0.2$, $D_0 = 0.1$, and $\hat{h}_1 = 1$.

5. Conclusion

A simplified approximate theoretical model for linear RTI system between EP solid and viscous fluid both with arbitrary thicknesses is presented in this paper. The model is with irrotational assumption and the velocity field is expressed with the velocity potentials. Although the solid constitutive relation has nonlinear characteristic which leads to be incapable to obtain analytical solutions for RTI in solids with EP transition by the previous velocity decomposition method, the model with the simplification in this work can deal with the viscosity, EP transition, and arbitrary thicknesses of both materials simultaneously with reasonable accuracy. The model treats thicknesses effects with boundary conditions in the irrotational velocity potentials and treats surface tension, fluid viscosity, and solid EP mechanical properties based on the continuity of velocity and force equilibrium at perturbation interface.

Applying the model in the RTI system of finite thicknesses fluids with viscosity and surface tension, the previous approximate dispersion relation deduced by the normal modes method is obtained again. Moreover, the analytical expressions of the interface amplitude motion equation, the growth rate and the instability boundary for the EP solid slab and finite thickness viscous fluid system are achieved, which can cover the cases with semi-infinite thicknesses by one-degree-of-freedom model based on the Newton second law.

The present study shows that the thicknesses of two materials unavoidably affect the instability evolution and reveals several features about thicknesses effect on the RTI system. For the plastic solid and viscous fluid interface, the growth rate is sensitive to the thickness of fluid. In addition, the thicknesses and A_T of two materials change the shape of the instability boundary and the stabilizing effect with increasing viscosity is stronger for low A_T than for high A_T.

References

[1] Bakhrakh S M, Drennov O B, Kovalev N P, Lebedev A I, Meshkov E E, Mikhailov A L, Nevmerzhitsky N V, Nizovtsev P N, Rayevsky V A, Simonov G P, Solovyev V P and Zhidov I G 1997 Lawrence Livermore National Laboratory Report No. UCRL-CR-126710 (unpublished)

[2] Dimonte G, Gore R and Schneider M 1998 *Phys. Rev. Lett.* **80** 1212

[3] Plohr B J and Sharp D H 1998 *Z. Angew. Math. Phys.* **49** 786

[4] López Cela J J, Piriz A R, Serna Moreno M C, Tahir N A and Hoffmann D H H 2006 *Laser Part. Beams* **24** 275

[5] Zhou Y 2017 *Phys. Rep.* **720–722** 1

[6] Zhou Y 2017 *Phys. Rep.* **723–725** 1

[7] Barnes J F, Blewett P J, McQueen R G, Meyer K A, and Venable D 1974 *J. Appl. Phys.* **45** 727

[8] Drucker D C 1980 *Mecha. Today* **5** 37

[9] Barnes J F, Janney D H, London R K, Meyer K A and Sharp D H 1980 *J. Appl. Phys.* **51** 4678

[10] Kalantar D H, Remington B A, Colvin J D, Mikaelian K O, Weber S V, Wiley L G, Wark J S, Loveridge A, Allen A M, Hauer A A and Meyers M A 2000 *Phys. Plasmas* **7** 1999

[11] Tahir N A, Deutsch C, Fortov V E, Gryaznov V, Hoffmann D H H, Kulish M, Lomonosov I V, Mintsev V, Ni P, Nikolaev D, Piriz A R, Shilkin N, Spiller P, Shutov A, Temporal M, Ternovoi V, Udrea S and Varentsov D 2005 *Phys. Rev. Lett.* **95** 035001

[12] McBride R D, Martin M R, Lemke R W, *et al.* 2013 *Phys. Plasmas* **20** 056309

[13] Kobyakov D and Pethick C J 2014 *Phys. Rev. Lett.* **112** 112504

[14] Gorczyk W and Vogt K 2015 *Gondwana Res.* **27** 196

[15] Opie S, Loomis E, Peralta P, Shimada T and Johnson R P 2017 *Phys. Rev. Lett.* **118** 195501

[16] Knapp P F, Martin M R, Dolan D H, Cochrane K, Dalton D, Davis J, Jennings C A, Loisel G P, Romero D H, Smith I C, Yu E P, Weis M R, Mattsson T R, McBride R D, Peterson K, Schwarz J and Sinars D B 2017 *Phys. Plasmas* **24** 042708

[17] Colvin J D, Legrand M, Remington B A, Shurtz G and Weber SV 2003 *J. Appl. Phys.* **93** 5287

[18] Remington B A, Allen P, Bringa E M, Hawreliak J, Ho D, Lorenz K T, Lorenzana H, McNaney J M, Meyers M A, Pollaine S W, Rosolankova K, Sadik B, Schneider M S, Swift D, Wark J and Yaakobi B 2006 *Mater. Sci. Technol.* **22** 474

[19] Park H S, Lorenz K T, Cavallo R M, Pollaine S M, Prisbrey S T, Rudd R E, Becker R, Bernier J V and Remington B A 2010 *Phys. Rev. Lett.* **104** 135504

[20] Sinars D B, Slutz S A, Herrmann M, *et al.* 2010 *Phys. Rev. Lett.* **105** 185001

[21] Sinars D B, Slutz S A, Herrmann M, *et al.* 2010 *Phys. Plasmas* **18** 056301

[22] Tahir N A, Hoffmann D H H, Kozyreva A, Tauschwitz A, Shutov A, Maruhn J A, Spiller P, Neuner U, Jacoby J, Roth M, Bock R, Juranek H and Redmer R 2000 *Phys. Rev. E* **61** 1975

[23] Hall C A, Asay J R, Knudsen M D, Stygan W A, Spielman R B, Pointon T D, Reisman D B, Toor A and Cauble R C 2001 *Rev. Sci. Instrum.* **72** 3587

[24] Tahir N A, Juranek H, Shutov A, Redmer R, Piriz A R, Temporal M, Varentsov D, Udrea S, Hoffmann D H H, Deutsch C, Lomonosov I and Fortov V E 2003 *Phys. Rev. B* **67** 184101

[25] Temporal M, Piriz A R, Grandjouan N, Tahir N A and Hoffmann D H H 2003 *Laser Part. Beams* **21** 609

[26] Miles J W 1966 General Dynamics Report No. GAMD-7335, AD 643161 (unpublished).

[27] Robinson A C and Swegle J W 1989 *J. Appl. Phys.* **66** 2859

[28] Swegle J W and Robinson A C 1989 *J. Appl. Phys.* **66** 2838

[29] Terrones G 2005 *Phys. Rev. E* **71** 036306

[30] Piriz S A, Piriz A R and Tahir N A 2017 *Phys. Rev. E* **96** 063115

[31] Mikaelian K O 1996 *Phys. Rev. E* **54** 3676

[32] Park H S, Lorenz K T, Cavallo R M, Pollaine S M, Prisbrey S T, Rudd R E, Becker R C, Bernier J V and Remington B A 2010 *Phys. Rev. Lett.* **105** 179602

[33] Piriz A R, López Cela J J and Tahir N A 2010 *Phys. Rev. Lett.* **105** 179601

[34] Piriz A R, López Cela J J, Cortázar O D, Tahir N A and Hoffmann D H H 2005 *Phys. Rev. E* **72** 056313

[35] Piriz A R, López Cela J J, Moreno M C S, Tahir N A and Hoffmann D H H 2006 *Laser Part. Beams* **24** 275

[36] Piriz A R, López Cela J J and Tahir N A 2009 *Phys. Rev. E* **80** 046305

[37] Piriz A R, Sun Y B and Tahir N A 2013 *Phys. Rev. E* **88** 023026

[38] Piriz A R, Sun Y B and Tahir N A 2014 *Phys. Rev. E* **89** 063022

[39] Sun Y B, Tao J J and He X T 2018 *Phys. Rev. E* **97** 063109

[40] Piriz A R, Piriz S A and Tahir N A 2019 *Phys. Rev. E* **100** 063104

[41] Bellman R and Pennington R H 1954 *Quart. J. Mech. Appl. Math.* **12** 151

[42] Piriz A R, Sun Y B and Tahir N A 2017 *Eur. J. Phys.* **38** 015003

[43] Gurtin M E and Anand L 2005 *J. Mech. Phys. Solids* **53** 1624

[44] Taylor G I 1950 *Proc. R. Soc. London Ser. A* **201** 192

[45] Landau L D and Lifshits E M 1987 *Fluid Mechanics*, 2nd edn. (Oxford: Pergamon)

[46] Chandrasekhar S 1961 *Hydrodynamics and Hydromagnetic Stability* (London: Oxford University Press)

[47] Landau L D and Lifshits E M 1986 *Theory of Elasticity*, 3rd edn. (Oxford: Pergamon)

[48] Piriz A R, López Cela J J and Tahir N A 2009 *J. Appl. Phys.* **105** 116101